

Mode-Switching of Active Droplets in Macromolecular Solutions

Prateek Dwivedi¹, Atishay Shrivastava¹, Dipin Pillai¹ and Rahul Mangal^{1*}.

¹Department of Chemical Engineering, Indian Institute of Technology Kanpur, Kanpur-208016, India

*Email: mangalr@iitk.ac.in

Abstract

Typical bodily and environmental fluids encountered by biological swimmers consist of dissolved macromolecules such as proteins or polymers, rendering them even non-Newtonian at times. Active droplets mimic the essential propulsive characteristics of several biological swimmers, and serve as ideal model systems to widen our understanding of their locomotive strategies. Here, we investigate the motion of a micellar solubilization induced swimming oil droplet in an aqueous medium consisting of polymers as macromolecular solutes. Experiments reveal extreme sensitivity of the droplet motion to the presence of macromolecules in its ambient medium. Through in-situ visualization of the self-generated chemical field around the droplet, we notice unexpectedly high diffusivity of the filled micelles in the presence of high molecular weight polymeric solutes. This highlights the breakdown of continuum approximation due to a significant size difference between the macromolecular solutes and the micelles. A modified and robust Peclet number framework is proposed that successfully captures the transition from smooth to jittery mode of propulsion for both molecular and macromolecular solutes. With an increase in macromolecular solute concentration, particle image velocimetry reveals another mode-switching from the conventional pusher mode to puller mode of propulsion, characterized by a more persistent droplet motion. By doping the ambient medium with suitable choice of macromolecules, our experiments unveil a novel route to orchestrate complex transitions in active droplet propulsion.

Introduction

The world of biological micro-organisms is strongly governed by the interactions between individual active agents and their immediate surroundings. These motile agents are capable of sensing, responding to, and in turn even altering the hydrodynamic and chemical fields around them. The ambient media around the microbial organisms thus critically shape their individual as well as collective behaviour. These media are often replete with diverse kinds of solutes, ranging in size from molecular to macromolecular solutes. For example, the ambient media may be imbued with macromolecular solutes such as proteins and enzymes that even render them viscoelastic. Also,

several bacterial species growing in aqueous media release an extracellular matrix such as exopolysaccharides, known to be crucial for their self-organization into colonies.¹ While this macromolecular ambient matrix acts as a physical and chemical shield to the bacterial inmates within, it also significantly affects the mode of propulsion characteristics, enabling quorum sensing, and crucially affecting the emergent growth of colonies. Biological micro-organisms such as bacteria, protozoa, cilia, sperm cells, etc. propel themselves utilizing specially designed microscopic appendages attached to their surface. They consume energy from their surroundings and exhibit extreme sensitivity to external stimuli including exposure to light, external flow, physical obstruction, and chemical impurities. To mimic their unique propulsion characteristics, several recent efforts have developed artificial swimmers. There are mainly two kinds of artificial swimmers a. Active particles (APs) and b. Active droplets (ADs). Self-propulsion in APs is achieved by generation of a physical/chemical gradient around the particle, through asymmetric interaction with the environment, a mechanism known as “phoresis”.² APs typically consist of Janus colloidal particles that rely on inherent asymmetry in their composition to produce the desired gradient, and propel themselves via self-diffusiophoresis,^{3,4} self-thermophoresis,⁵ or self-electrophoresis.^{6,7} ADs, on the other hand, utilize either a chemical reaction or micellar solubilization to drive the motion of isotropic droplets of one fluid in another immiscible fluid. The surface tension gradient driven Marangoni flow is at the heart of self-propulsion in ADs. These artificial swimmers have been demonstrated to not only mimic microbial motion but also their response to external impetus through phenomena such as chemotaxis,^{8,9} rheotaxis,^{10–13} and gravitaxis.¹⁴

Different propulsion strategies include interfacial reaction,^{15–17} phase separation,¹⁸ and micellar solubilization.^{8,19–21} Among these, owing to its simplicity and non-reactive nature, micellar solubilization is the most popular to generate stable, sustained propulsion in droplets. When the surfactant concentration is significantly higher than its critical micelle concentration (CMC), micellar solubilization spontaneously generates an interfacial tension gradient along the interface. The resultant Marangoni stress causes the fluid at the interface from the region of low to high interfacial tension, driving the droplet in the opposite direction. Using a convection-diffusion model for the migration of the chemical entities, Morozov and Michelin²² theoretically proposed that an increase in Peclet number (Pe) forces the droplet to strongly interact with its own chemical field leading to a transition from smooth to jittery motion. The transition was proposed to be a consequence of the onset of higher hydrodynamic modes resulting from an increase in Pe . Experimental studies, where either the surfactant concentration was increased²¹ or non-reactive solutes were added¹⁹ verified their proposed change in motion. In 2021, using a combination of

experiments and linear stability theory, Suda *et al.*²³ proposed a size-dependent transition from straight to curvilinear motion. However, considering the difference in the physicochemical complexity of different experimental systems, the underlying physics responsible for Pe induced transition, is still not explicitly clear. Furthermore, considering the long-term application of artificial droplets where they can be used to perform intricate tasks in microfluidic domains in fluids with a variety of chemical species, understanding the effect of the chemical complexity of the surrounding environment, in particular those which render viscoelasticity to the environment, is even more crucial. The role of macromolecular solutes in modifying microbial propulsion therefore warrants a detailed investigation. In this work, we investigate the dynamics of active droplets in the presence of polymeric solutes with varying molecular weights and concentrations.

In this study, we consider 4-pentyl-4'-cyano-biphenyl (5CB) oil droplets dispersed in an aqueous solution of tetradecyltrimethylammonium bromide (TTAB) surfactant. The droplets self-propel via micellar solubilization.^{8,19} Unlike molecular solutes, the addition of high molecular weight polymeric solutes did not lead to any jittery motion. Through in-situ visualization of the trail of filled micelles left behind by the droplet, we show that diffusion of filled micelles is critical in determining the onset of the jittery dynamics of the droplet. A hierarchical mode-switching from a smoothly propelling puller to pusher mode, followed by a transition to jittery mode, is shown to be characterized by a modified Peclet number Pe^* , which explains all the previous and present observations.

Materials and Methods

Chemicals. 4-Cyano-4'-pentylbiphenyl (5CB) was procured from Sigma Aldrich, trimethyl ammonium bromide (TTAB) and glycerol were procured from Loba chemicals, Polyethylene Glycol of M_w 's ~ 35, 100, 600, 1000 and 8000 kDa were procured from Sigma Aldrich. All the chemicals were used as procured. For PIV analysis, red dyed aqueous fluoro spheres of size 500 nm was procured from Thermo ScientificTM. Oil soluble fluorescent dye 'Nile Red' was procured from Sigma Aldrich.

Sample preparation. We dispersed 5CB droplets in aqueous solution of 6wt% TTAB. Different samples were prepared by adding glycerol, and PEG of different M_w 's to the aqueous solution of TTAB as solutes. 5CB droplets of size ~80 μm were generated using a micro-injector (Femtojet 4i, Eppendorf) by injecting appropriate amount of nematic liquid crystal 5CB into 6 wt% aqueous solution of TTAB surfactant and solutes (glycerol and polymers). To ensure low number density of droplets to avoid droplet-droplet interaction, low concentration of 5CB, ~ 0.15 v/v%, was used. The

emulsion was then injected into a custom-made Hele-Shaw type optical cell (vertical gap of 100 μm), prepared using cleaned (ultrasonicated in ethanol followed by plasma treated and nitrogen dried) glass slides. Fresh optical cells were used for every sample.

Rheology measurements. To measure the variation of bulk viscosity (η_b) vs shear rate ($\dot{\gamma}$) of different fluids, flow sweep shear rheology experiments were performed. Host polymer relaxation time (τ) was obtained from the cross-over of storage modulus $G'(\omega)$ and loss modulus $G''(\omega)$, measured using frequency sweep measurements at strain (γ) of 1%. All the measurements were performed at 25 °C in a rheometer (TA Instruments DHR3) fitted with a Couette assembly.

Droplet visualization and tracking. To visualize motion of isolated active droplets, the optical cell was placed on a temperature stage mounted on an upright polarized optical microscope Olympus BX53. The temperature stage was used to maintain target temperature of the sample. Olympus LC30 camera with 2048 x 1532 pixels resolution was used in brightfield mode to capture the motion of the droplets. Droplet tracking was performed with Image-J software which utilizes an image correlation-based approach to obtain particle trajectories (X (μm), Y (μm)) vs. elapsed time (Δt). A rheometer (TA Instruments DHR3) with a couette assembly was used to measure the viscosity of the aqueous solutions with different solutes

Fluorescence experiments. For observation of chemical field around the droplet, oil soluble fluorescent dye (Nile Red) was dissolved in 5CB oil. Laser of wavelength ~ 560 nm was used to excite the dye molecules. For obtaining hydrodynamic field around the droplet, surrounding aqueous solution was doped with red fluorescent tracers (500nm Polystyrene particles) particle image velocimetry (PIV) experiments were performed. During the fluorescence experiments, ORX-10G-71S7C-C, FLIR, camera with 3208 x 2200 pixels was used with constant exposure throughout the video.

Results & Discussion

For the purpose of benchmarking our experimental setup, we begin by reproducing well-established observations of active droplets (~ 80 μm) in an aqueous solution of TTAB, first devoid of any solute, and subsequently with glycerol added as a molecular additive. In the absence of any solute, the droplets perform expected smooth ballistic motion (with propulsion speed ~ 20 -50 $\mu\text{m s}^{-1}$) at small times and random motion at long times. The trajectory expectedly demonstrates traces of curling behavior due to the nematic phase of the droplet.²⁴ Since the density of 5CB ($\rho_{5CB} \sim 1.057$ g ml^{-1}) is

higher than water ($\rho_{water} \sim 0.99 \text{ g ml}^{-1}$), the droplets remain confined in the 2D (X-Y) plane close to the bottom wall of the optical cell and move with negligible vertical (Z) drift, again consistent with previous reports^{8,25}. Further, with the addition of glycerol as solute ($c_{solute} = c_{Glycerol} = 94\text{wt}\%$), recent experimental reports^{19,26} are reproduced, wherein the droplet exhibits short-time jittery and long-time random motion. Although $\rho_{Glycerol}$ ($\sim 1.25 \text{ g ml}^{-1}$) is greater than ρ_{5CB} ($\sim 1.057 \text{ g ml}^{-1}$), the vertical height of the optical cell being comparable to the droplet size ensures that the droplets primarily remain confined in the 2D plane.

Having benchmarked our experimental setup, we proceed to systematically investigate the effect of macromolecular solutes on droplet self-propulsion. To this effect, polyethylene glycol (PEG), as a macromolecular additive, of different molecular weights (M_w) is added to the aqueous surfactant solution. The concentration of the various M_w PEG added was adjusted such that the bulk viscosity (η_b) of the ambient fluid in all cases was matched. It is to be noted that for all polymeric samples, $c^* \ll c_{PEG} \ll 1$, suggesting a semi-dilute regime. Here, $c^* = \frac{3M_w}{4\pi R_g^3 N_A}$ is the overlap concentration, $R_g = 0.02M_w^{0.588}$ is the radius of gyration of PEG in good solvent (e.g. water), and N_A is the Avogadro number.

Motility in Viscous Macromolecular Media

The addition of macromolecular solutes to the ambient medium may potentially affect the bulk viscosity, species diffusivity as well as introduce viscoelastic effects in the medium. Since the motility of active droplets is sensitive to both the chemical and hydrodynamic fields in the ambient medium, it is important to isolate the effects of various physics. We thus begin with a discussion of the experiments wherein the addition of macromolecules do not introduce any noticeable elastic effects in the ambient medium, i.e., Deborah number (De) = $\frac{\tau R}{V} \ll 1$. Here, τ is the polymer relaxation time, V is the droplet speed, and R is the droplet radius. The role of macromolecules in such systems is therefore limited to altering the bulk viscosity of the ambient medium as well as surfactant diffusivity. The latter effect on surfactant diffusivity is of particular significance and shall be elaborated upon later. The composition and physical properties of the ambient medium in the presence of different solutes are provided in Table 1. As seen from the table, Fluid 1 represents the ambient medium devoid of any solute, while Fluid 2 is 94 wt% glycerol. Fluids 3 to 7 represent the ambient medium added with PEG of increasing molecular weight, ranging from 35 kDa to 8000 kDa.

Table 1: Composition and physical properties of the ambient medium consisting different solutes.

Fluid	Solute	M_w (kDa)	c_{solute} (wt%)	η_b (Pa-s)	dR/dt ($\mu\text{m min}^{-1}$)
1	NA	NA	NA	0.001	0.57
2	Glycerol	NA	94	0.32	1.50
3	PEG	35	25	0.29	0.54
4	PEG	100	15	0.45	0.46
5	PEG	600	3	0.40	0.30
6	PEG	1000	2	0.37	0.33
7	PEG	8000	0.5	0.37	0.32

Figure 1(A) shows typical trajectories (captured for $\sim 180\text{s}$) of active 5CB droplets swimming in different ambient media listed in Table 1. Clearly, for low M_w PEG as solute (fluid 3), the motion of the active droplet is jittery and qualitatively similar to that of glycerol as solute (fluid 2). With slightly higher M_w PEG (fluid 4), jitteriness in the motion is slightly suppressed. For three high M_w PEG solutes (fluid 5, 6 and 7), the motion is smooth and similar to that in the absence of any solute (fluid 1). In figure 1(B), we plot the variation in the persistence length, $L_p = \langle v \rangle \tau_R$, of the trajectories

of active droplets in different fluids. $\langle v \rangle = \frac{|\mathbf{r}_{i+1} - \mathbf{r}_i|}{t_{i+1} - t_i}$ is the average propulsion speed, where $\mathbf{r}_i = (\mathbf{X}(t_i), \mathbf{Y}(t_i))$ and τ_R is the rotational time scale of the droplets, respectively. τ_R is computed using the temporal decay of the velocity autocorrelation data $C(\Delta t) = \langle \mathbf{v}_{inst.}(\Delta t) \cdot \mathbf{v}_{inst.}(0) \rangle$ (see supporting figure S1). Systems with smooth droplet motion exhibits large L_p , whereas with increasing jitteriness, L_p decreases.

The bulk viscosity (η_b) of the different ambient media and the corresponding rate of solubilization (dR/dt) of active droplets in them are listed in table 1. The bulk viscosity was determined using flow-sweep shear rheology measurements. The data in table 1 suggest that neither dR/dt nor η_b of the ambient media in isolation correlates with the observed transition from smooth to jittery motion. Past studies, however, have attributed either bulk viscosity²⁷ or the enhanced rate of solubilization¹⁹ to explain such a transition. The theoretical model by Morozov and Michelin²⁸ predicts a transition from smooth to jittery motion if the Peclet number ($Pe = \frac{Rv_t}{D}$) exceeds significantly beyond the critical threshold. They showed that as convection dominates diffusion, the emergence of higher modes of convection may result in a transition from steady propulsive state to a transient chaotic motion. In the above, R is the droplet radius and v_t is the characteristic velocity scale given by the terminal velocity of the droplet under the combined influence of diffusiophoretic and Marangoni effects. Some studies have used D as the diffusion coefficient of the surfactant monomer,^{22,29} whereas, others have reported D as the diffusion coefficient of the micelles.^{20,30} Using the

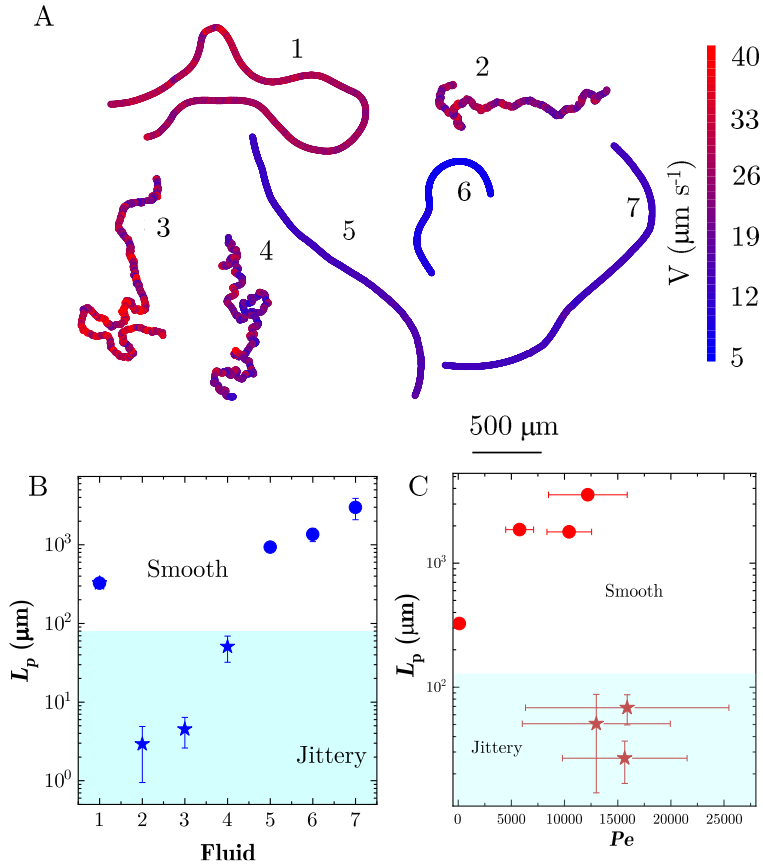


Figure 1: (A) Representative trajectories ($\sim 180\text{s}$) of active 5CB droplets in different media listed in table 1. (B) Variation in L_p with fluid type. (C) Variation in L_p with Pe .

experimentally measured maximum instantaneous speed of the droplet v_{\max} as the characteristic velocity scale, and bulk viscosity η_b to compute micelle diffusivity via the Stokes-Einstein equation, $D = \frac{k_b T}{6\pi\eta_b a}$, we determined Pe for active droplets in the different ambient media. Figure 1C shows the variation of L_p with Pe , which again reveals no correlation between Pe and the transition from smooth to jittery motion for macromolecular solutions. We show that this discrepancy may be attributed to the size of macromolecular solutes, i.e., polymers, affecting the diffusivity of filled micelles.

In order to experimentally measure the micelle diffusivity D , the droplet phase was doped with a hydrophobic fluorescent dye (Nile Red, Sigma Aldrich) and excited using a laser light of 560 nm wavelength. This facilitated the visualization of the concentration field associated with the trail of filled micelles released by the droplets during their self-propulsion (Figure 2A). The spread of this trail in the direction perpendicular to droplet motion is indicative of the diffusion of filled micelles.

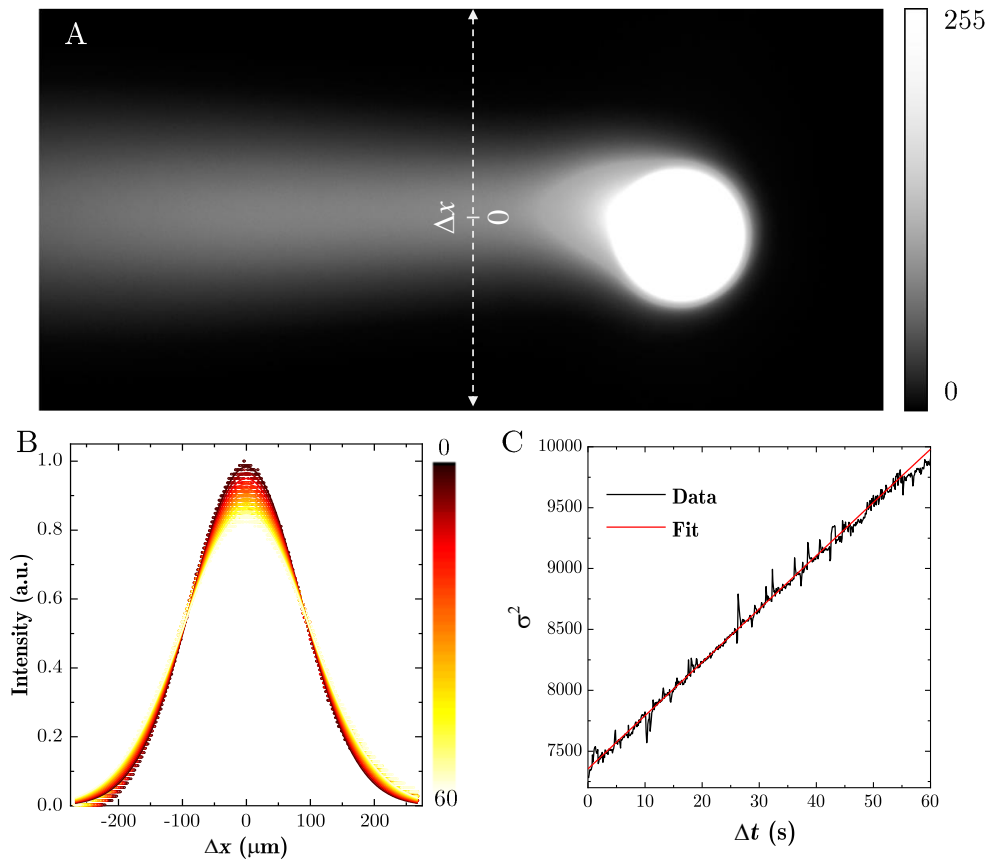


Figure 2: (A) Fluorescence micrograph (greyscale) of an active 5CB droplet leaving a trail of filled micelle around it. (B) The time evolution of fluorescent intensity along the dashed line shown in (A) overlaid by the Gaussian fits. (C) Temporal change in the variance (σ^2) of the Gaussian fit shown in (B). The solid line represents a linear fit.

To avoid the oversaturated signal at the droplet, we extract the intensity ($I(x, \Delta t)$) of the fluorescence at a distance $\sim 4R$ from the droplet center in its wake, at different times, along a line perpendicular to the droplet motion (Figure 2B). As shown in the figure, $I(\Delta t)$ expectedly shows a Gaussian profile, which can be fitted using the following equation:

$$I(x, \Delta t) = \frac{M_o}{\sqrt{4\pi D\Delta t}} \exp\left(\frac{-x^2}{4D\Delta t}\right) \dots\dots\dots(1)$$

$$\text{where, } M_o = \int_{-\infty}^{\infty} I(x, 0) dx \dots\dots\dots(2)$$

The Gaussian curve-fitting suggests that the spatial variance increases linearly with time (Δt), given by $\sigma^2 = 2D\Delta t$ (figure 2C), whence the filled micelle diffusivity, D , can be determined. Figure 3A depicts the variation of D/D_{SE} for the filled micelle in different ambient media, wherein $D_{SE} = \frac{k_B T}{6\pi\eta_b a}$ is the theoretical Stokes-Einstein diffusion coefficient. Here, k_B is the Boltzmann constant, T is the temperature, a is the micelle size (~ 5 nm), and η_b is the bulk viscosity of the ambient medium. The plot indicates that for polymeric solutions with large molecular weight PEG, the experimentally measured D is much larger, approximately 2 orders of magnitude higher than the expected D_{SE} . This positive deviation in diffusivity of the filled micells is reminiscent of superdiffusivity observed for nanoparticles (NPs) of the size ~ 5 -10 nm in polymeric melts/solutions. It is well-established that such a superdiffusive phenomenon arises due to the significant size difference between the NPs and the polymer chains in the suspending medium.³¹⁻³⁵ When the size of dispersed NPs is smaller or equivalent to the polymer length scale, the continuum hypothesis breaks down. Owing to their relative smaller size, NPs do not experience the bulk-scale drag offered by the polymer chains characterized by η_b . Instead, the diffusion of NPs is mainly governed by the local viscosity (η_{local}), which depending on the size disparity can be significantly lower than η_b , even approaching the solvent viscosity, i.e., η_{water} , in the limiting case. As mentioned earlier, since our polymeric solutions are in the semi-dilute regime, the relevant characteristic polymeric length scales are the correlation length $\xi = b\phi^{-0.76}$ and the tube diameter $d_t = b\sqrt{N_e}\phi^{-0.76}$ for the case of good solvent.^{31,36} Here, the

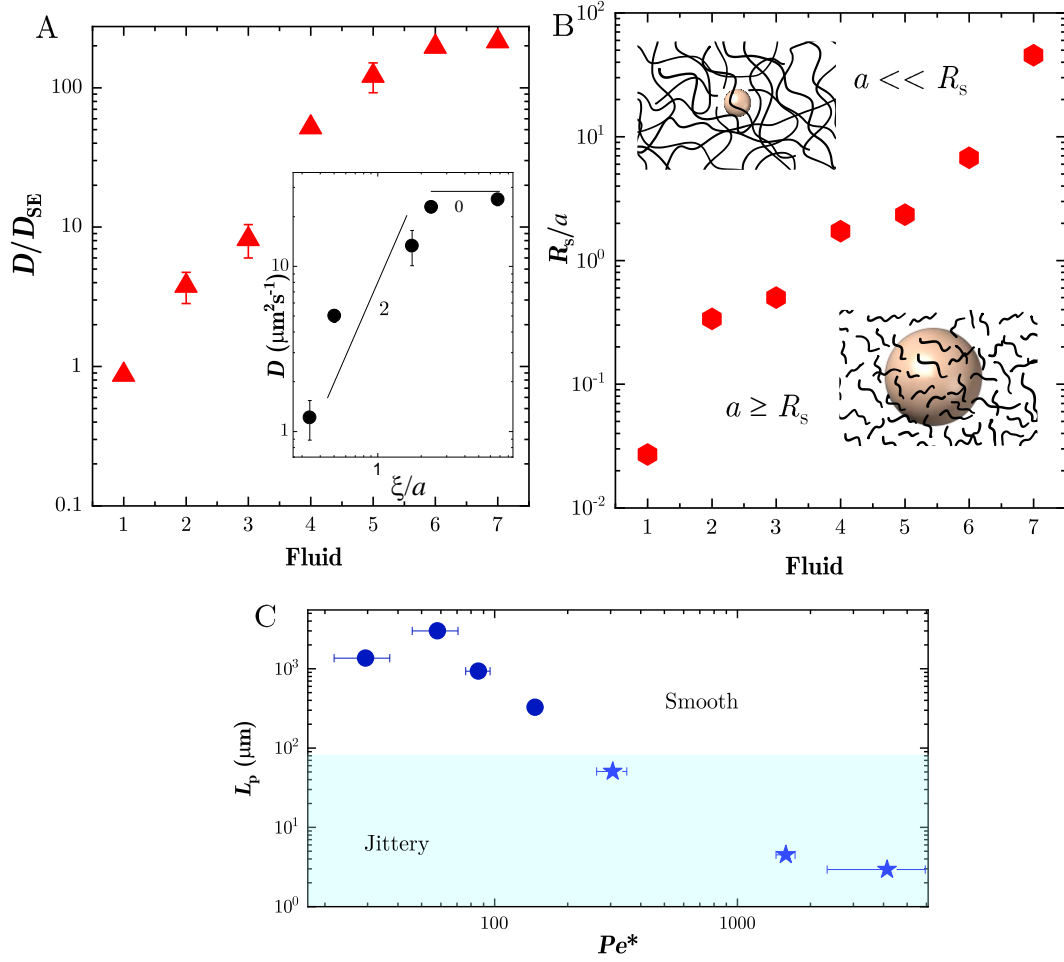


Figure 3: (A) Variation of D/D_{SE} for filled micelles in different ambient media. The inset shows the variation of D with ξ/a for the macromolecular solutions. (B) Variation in R_s/a with fluid type. Insets depict the schematic of micelle in the small size and intermediate size range. (C) Variation in L_p with Pe^* .

volume fraction $\phi = c_{PEG}/\rho_{PEG}$, $\rho_{PEG} = 1.125 \text{ gm ml}^{-1}$ is the PEG density and $b = 1.1 \text{ nm}$ is the length of a Kuhn segment for PEG chains. These two length scales have been listed in table 2 for the different ambient media.

Table 2: Characteristic length scales for different polymeric solutes.

PEG M_w (kDa)	c_{solute} (wt%)	ξ (nm)	d_t (nm)
35	25	3.37	9.97
100	15	5.02	17.02
600	3	17.24	58.46
1000	2	23.48	79.62
8000	0.5	67.43	228.65

Based on the scaling law proposed by Cai *et al.*³¹, we expect that micelles in small size range ($a < \xi$) are effectively dragged by the local solvent viscosity ($\eta_{local} = \eta_{water}$) suggesting $D \sim k_B T / \eta_{water} a$. For intermediate sized micelles ($\xi < a < d_t$), the effective local viscosity experienced by the micelles is proportional to the number of correlation blobs in a polymer chain section with size of the order of particle diameter ($\eta_{local} = \eta_{water} \left(\frac{\xi}{a}\right)^{-2}$), suggesting $D \sim \frac{k_B T}{\eta_s a} \left(\frac{\xi}{a}\right)^2$. Figure 3B shows the variation in the ratio of solute characteristic length scale to micelle size R_s/a for different fluids. Here R_s equals the molecular size for glycerol in the case of fluid 2, and $R_s = \xi$ as listed in table 2 for macromolecular fluids 3 to 7. As discussed earlier, due to the large size disparity between the micelle and the high Mw PEG solutes, we expect the continuum hypothesis to fail, leading to a much faster micelle diffusivity. The inset of figure 3A depicts the variation of experimentally measured D for micelles in polymeric solution with ξ/a . We find that the scaling of D with ξ/a agrees with the scaling law predicted by Cai *et al.*³¹, confirming that the motion of micelles is governed by the local visous drag. Next, using the experimentally measured D for the micelles which captures the effect of η_{local} , we compute a modified Pe^* . Figure 3C displays the variation in L_p with Pe^* , where a monotonic decrease in L_p with increasing Pe^* is evident, in agreement with the extant theoretical predictions. For smaller Pe^* , micelle diffusion dominates advection leading to a sustained motion in a particular direction. However, for larger Pe^* , advection of filled micelles becomes prominent compared to diffusion, forcing the droplet to interact with the self-generated chemical field. This causes the droplet to change direction frequently, with intermittent stopping, leading to jittery motion. Our study suggests that the validity of conventional Pe , defined in terms of Stokes-Einstein diffusivity is limited to molecular solutes only, wherein the size of a micelle is similar to the size of the added solute and so the viscosity experienced by the micelle equals η_b . Whereas for macromolecular solutes such as polymers, due to the significant size difference between the micelles and the solutes, a modified framework of Pe^* where D is defined using η_{local} should be used. This accurately captures the enhanced diffusion of micelles in macromolecular solutions and therefore the jittery transition as well. In the limiting case of molecular solutes, $\eta_{local} = \eta_b$, and thus yields $Pe^* = Pe$, thus rendering the Pe^* as the universal parameter that characterizes the transition from smooth to jittery motion for all kinds of solutes, whether molecular or macromolecular.

Motility in Weakly Viscoelastic Macromolecular Media

So far, we limited our discussion to Newtonian ambient media ($De = 0$), allowing us to solely investigate the effect of change in molecular weight of macrosolutes or η_{local} , on the motion of the active droplets. Now, to explore the effect of viscoelasticity, the motion of various ~ 80 nm active droplets is investigated in ambient media with 8000 kDa PEG at varying concentrations (c_{PEG}). The

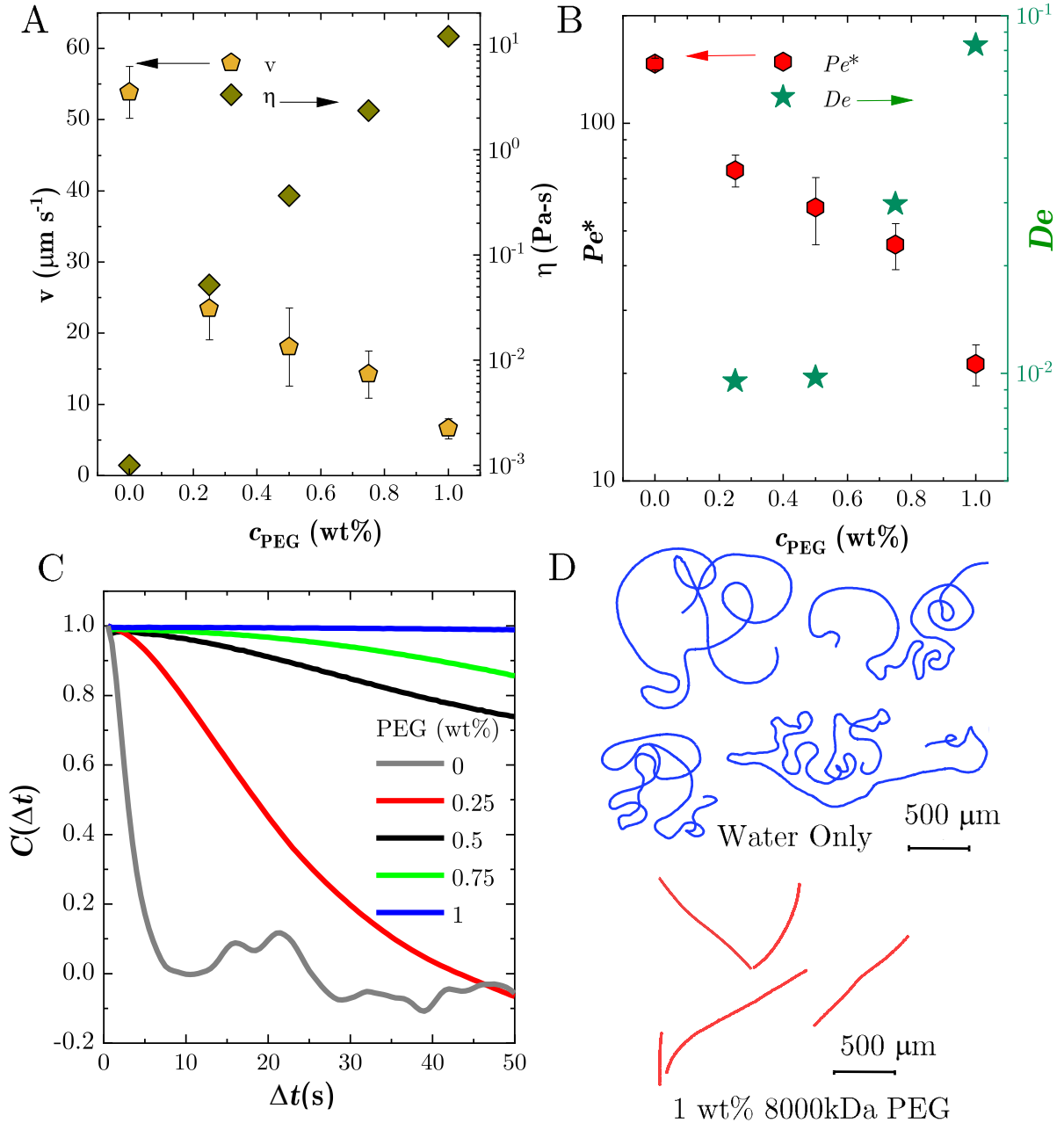


Figure 4: For active droplets in polymeric solutions with 8000 kDa PEG at different concentrations c_{PEG} (A,B) Variation in propulsion speed v , bulk viscosity η , Pe^* and De with c_{PEG} . (C) Velocity autocorrelation $C(\Delta t)$. (D) Few representative trajectories (~ 200 s) comparing the persistent motion of active 5CB droplets in polymeric samples with $c_{PEG} = 0$ wt% (blue) and $c_{PEG} = 1$ wt% (red).

relaxation time (τ) and bulk viscosity (η_b) of these polymeric solutions were measured from the oscillatory shear rheology experiments. Figure 4A shows an increase in η_b and a consequent decrease in the droplet speed v with an increase in c_{PEG} . In these systems, since the surfactant concentration is kept the same ($c_{TAB} = 6\text{wt}\%$) it results in a nearly unchanged rate of solubilization dR/dt ($\sim 0.3 \text{ mm min}^{-1}$), and since the polymer characteristic length scale ξ ($\sim 50 \text{ nm}$) is greater than the micelle size ($\sim 10 \text{ nm}$), D also remains nearly the same ($\sim 24 \mu\text{m}^2 \text{ s}^{-1}$). It is therefore noteworthy that despite a 10^4 times increase of η_b for $c_{PEG} = 1\text{wt}\%$, compared to water, the reduction in droplet speed is nearly 1/10 only. In 2012, using numerical simulations Zhu *et al.*³⁷ investigated the swimmers with different swimming gaits in polymeric solutions and predicted that the polymers in the fluids can transfer the stored mechanical energy, gained due to deformation, to the swimming droplet making the swimming more efficient compared to the Newtonian fluids.

With an increase in c_{PEG} , a dramatic increase in η_b results in a decrease in Pe^* (figure 4B). Also, despite a decrease in v , a stronger increase in τ with increase in c_{PEG} results in an increase in De (figure 4B). Figure 4C demonstrates slower decay in velocity autocorrelation $C(\Delta t)$ with increasing c_{PEG} suggesting more persistent motion in viscoelastic solutions. A comparison of a few representative trajectories captured for active droplets swimming in just water and in 1wt% 8000kDa PEG solution, has been shown in figure 4B, which highlights the more linear trajectories in the latter. More persistent motion with decrease in Pe^* is consistent the diminished effect of advection and diffusion of filled micelles becoming more important. Using water in oil emulsion Suda *et al.*²³ recently reported that on increasing droplet size, the droplet motion becomes more curvilinear, indirectly suggesting that low Pe is associated with more persistent motion. Suda *et al.* also reported a transition in swimming mode from puller to pusher, on increasing droplet size (increase in Pe), which was accompanied by straight-to-curvilinear transition. The pusher mode was demonstrated to be more susceptible to perturbations, where the higher swimming modes become dominant leading to change in swimming direction.

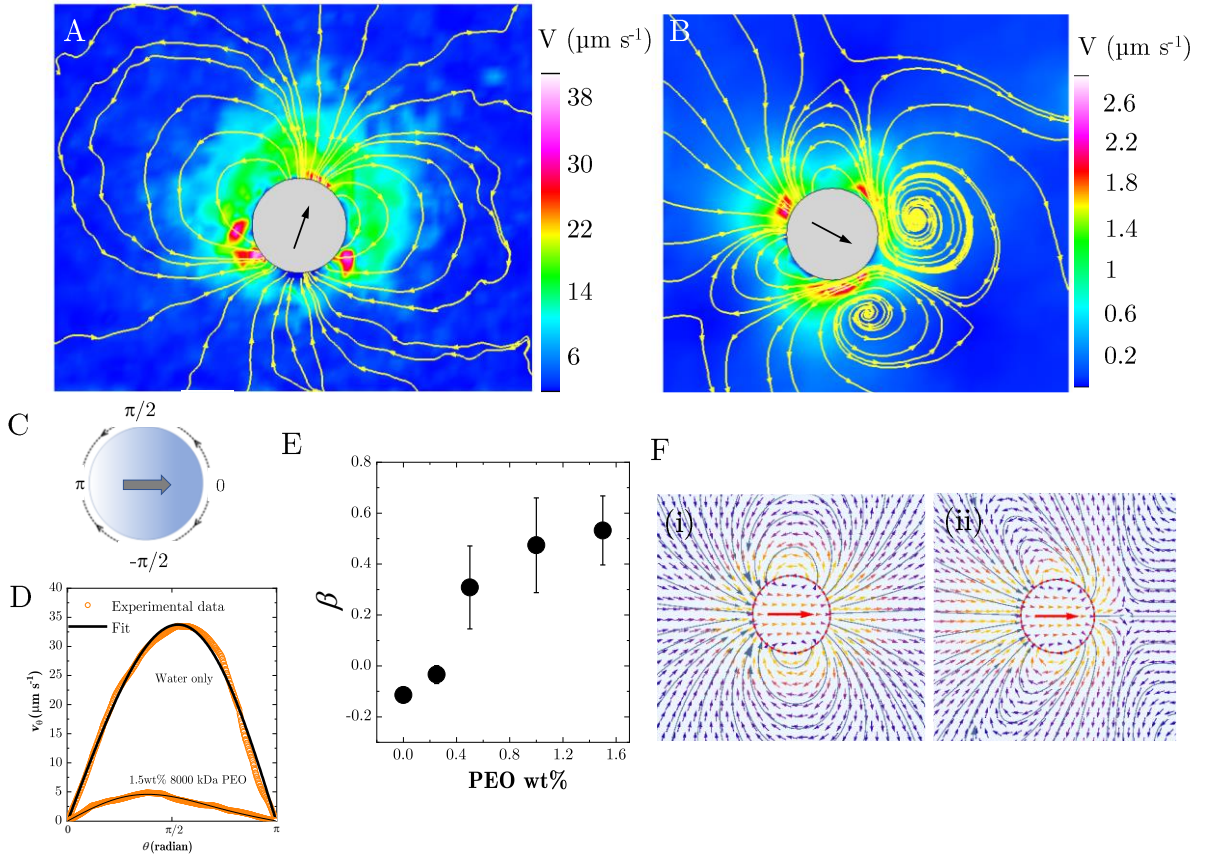


Figure 5: (A-B) Fluorescent micrographs depicting streamlines obtained from PIV measurements. The streamlines represent the flow-field around the droplet. (A) is for droplet motion in just water ($C_{PEG}=0$ wt%) where the droplet appears to be a weak pusher. (B) corresponds to droplet motion in ($C_{PEG}=1.5$ wt%) where it appears to be a puller. C. Schematic of the tangential velocity field around an active droplet. (D) Tangential flow velocity, obtained from PIV measurements, at the droplet interface, in the comoving frame of reference. Black lines are fits to Eq. (3). (E) β obtained from the fitting as a function of C_{PEG} . (F) Theoretical flow profile using the squirmer model (39) for (i) a weak pusher active droplet with $\beta = -0.05$, (ii) a puller active droplet with $\beta = 0.5$.

To probe the swimming mode of the active droplets in our experiments, we also performed particle image velocimetry (PIV) measurements to estimate the flow field around the active droplets. The streamlines of the flow-field in the laboratory frame for droplets in the solution with $c_{PEG}=0$ wt% and $c_{PEG}=1.5$ wt% are shown in figure 5A-B. The flow-field around the active droplet (Figure 5A) has streamlines being pushed away from the droplet apex, with the maximum speed in the posterior hemisphere of droplet, thus exhibiting a pusher mode of swimming. In contrast, the droplet moving in 8000kDa PEG aqueous solution with $c_{PEG}=1.5$ wt% has streamlines being pulled in from the front (Figure 5B) with maximum speed in the anterior hemisphere of droplet, thus exhibiting a puller

mode of swimming. The PIV data was used to compute the tangential velocity at the droplet interface $u(R, \theta)$ in the co-moving frame of reference (Figure 5C). The tangential velocity at $r = R$ is expressed

as $u(R, \theta) = \sum_{n=1}^{\infty} B_n V_n(\cos \theta)$, where $V_n(\cos \theta) = \frac{2}{n(n+1)} \sin \theta P_n'(\cos \theta)$, and P_n is the Legendre polynomials

^{38,39}. A manageable and relevant formula is obtained by assuming $B_n=0$ for $n > 2$, resulting in

$$u(R, \theta) \sim B_1 \sin \theta + \frac{B_2}{2} \sin 2\theta \dots \dots (3)$$

The ratio, $\beta = \frac{B_1}{B_2}$, determines the nature of the swimming mode. For pusher $\beta < 0$, for neutral $\beta = 0$

and for puller $\beta > 0$ ⁴⁰. The theoretical velocity profile obtained by solving the squirmer model³⁹ is

depicted in figure 5F for two prescribed values of β , viz., (i) $\beta = -0.05$ and (ii) $\beta = 0.5$. These

correspond to the values determined experimentally for the profiles shown in figures 5A and 5B

respectively. It can be seen that the experimental and theoretical profiles are in good qualitative

agreement. Figure 5E reveals an increase in β with c_{PEG} , marking a mode-switching from pusher to

puller mode of propulsion with increasing c_{PEG} . This novel pusher to puller transition at first appears

to be due to an increase in the viscoelasticity, i.e., increase in De . However, as shown in figure 4B,

an increase in c_{PEG} also results in a decrease in Pe^* , suggesting this to be an advection-diffusion

induced transition, so far known for Newtonian media. To establish this, we perform additional

experiments with concentration of 4wt% and 5wt% of relatively low molecular weight of 600 kDa

PEG to achieve low Pe^* at very low De . Under these conditions, the droplet exhibits a puller mode,

confirming that the pusher to puller transition is marked by a decrease in Pe^* . It is important to

note here that the pusher to puller transition with decreasing Pe^* so far has not been predicted by

the extant theories/numerical simulations. Very recently Li ⁴¹ theoretically reported unsteady droplet

motion of mixed pusher–puller modes along zig-zag trajectories. However, the prediction was made

for the highly non-linear regime, i.e., at high Pe^* . It was demonstrated that the interaction between

the primary wake and the secondary wake of low surfactant concentration leads to this unusual

dynamic swimming mode. Experimentally, so far pusher to puller transition for swimming oil

droplets in aqueous surfactant solution has not been reported yet. As mentioned earlier, for water in

oil droplet system, Suda *et al.* reported the existence of puller mode at low Pe , the underlying physics

for which is expected to be similar to ours, but the exact mechanism is largely elusive. One possible

reason for not observing a puller mode in aqueous medium devoid of macromolecules could be the

challenging experimental conditions in achieving low enough Pe^* . Our work presents a novel route

using macromolecules to increase the bulk viscosity without altering the local micelle-scale viscosity

to achieve low enough Pe^* with ease and explore a regime which, so far, was inaccessible for oil in water emulsions (Suda *et al.* reported this transition for oil in water emulsion). In 2015, Carato *et al.*⁴² used a regular perturbation analysis (expansion in De) to assess the role of weak viscoelasticity on different squirming modes in a weakly second-order fluid. The study demonstrated that in Newtonian fluids, neutral squirmers are the most efficient. However, with an increase in ambient viscoelasticity, even weakly, pullers dissipate lesser energy and hence are more efficient. In our experiments with no added solutes, the droplet was a weak pusher mode ($\beta \sim -0.1$), which is close to being a neutral swimmer. Further, adding slight viscoelasticity to the ambient medium (increasing De) resulted in a puller mode of propulsion, which is consistent with the predictions of Carato *et al.* With the help of more experimental and theoretical efforts, the exact underlying physics still needs to be fully understood. Finally, exploring the validity of higher order transitions (puller to pusher to quadrupole) at higher Pe^* for viscoelastic ambient media, so far known for Newtonian fluids, is also extremely pertinent. So, we repeated the investigation of the motion of active 5CB droplets in different viscoelastic solutions at higher $c_{TTAB} \sim 15$ and 30wt%, where droplets performed smooth motion with pusher mode at 15wt% and jittery motion with quadrupole mode at 30wt%. This confirms that even at $De > 0$, increasing Pe^* results in puller to pusher to quadrupole transition. We

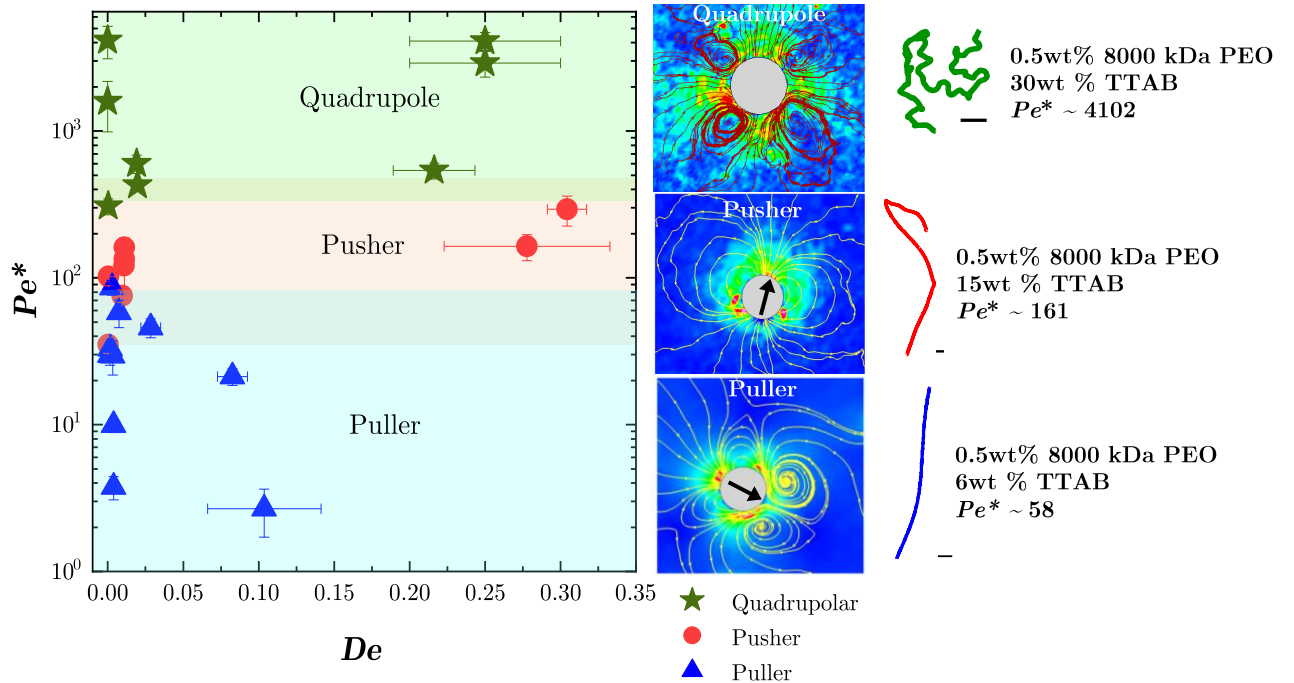


Figure 6: Phase diagram between Pe^* and De , mapping the different modes of droplet swimming under various ambient media. Next to the phase diagram are the fluorescent micrographs depicting streamlines obtained from PIV measurements for the three swimming modes and the corresponding X-Y trajectories (scale bar 50 μm) captured for $\sim 75\text{s}$.

summarize the hierarchical mode-switching (puller-to-pusher-to-jittery) in droplet propulsion for the various ambient media considered in this study using a phase diagram plotted between Pe^* and De . Although constructing a detailed phase diagram needs more careful experiments and analytical predictions, our experimental findings strongly highlight that the known Pe^* based transition of swimming for Newtonian fluids, is valid for viscoelastic solutions as well, and the addition of viscoelasticity does not alter this transition.

Conclusion and Summary

We studied self-propelled motion of droplets in polymer-doped aqueous media. By probing the 2D motion of these droplets, it was shown that with increasing molecular weight of the polymer chains, the droplet trajectories became more persistent. Through fluorescent microscopy, it was demonstrated that in polymeric solutions, the micelle diffusivity (D) is much faster than the theoretical expectation (SE equation) based on the bulk viscosity, and hence the conventional Pe where D is estimated using η_b does not explain the transition. A modified Pe^* framework that utilizes the micelle diffusivity based on the local viscosity of the surrounding environment was demonstrated to capture the transition appropriately. Using particle image velocimetry (PIV), we demonstrated that for high molecular weight polymers, on increasing the polymer concentration, the swimming mode of the active droplets switches from pusher to the puller. Such transitions have never been reported for artificial droplets. On further changing the Pe^* using the surfactant concentration, a second transition from pusher to quadrupole was also demonstrated. Our observations suggest that on careful adjustment of the Pe^* and De , the transitions of swimming droplets between different modes pusher/puller/quadrupole can be manipulated. We foresee that with synchronous efforts from both experiments and theory/simulations, a detailed phase space can be constructed, which will be of huge interest in understanding the diverse range of active motions observed in nature.

Acknowledgments

This work is supported by the Science and Engineering Research Board (SB/S2/RJN-105/2017), Department of Science and Technology, India. We also thank Dr. Shashi Thutupalli and Dr. Rajesh Singh for insightful discussions on our work.

Author Contributions: PD and RM conceptualized the research, PD & RM designed the methodology of the experiments, PD performed the experiments, PD, AS and RM analyzed the experimental data, PD, DSP and RM wrote the paper.

Competing Interest Statement: Authors declare no competing interest.

References

- (1) Ward, B. A. J. I. The Kinetics of Oil Solubilisation in Aqueous Surfactant Solutions Author (s): Anthony J. I. Ward Source : Proceedings of the Royal Irish Academy . Section B : Biological , Geological , and Published by : Royal Irish Academy Stable URL : [Http://Www.Js. 1989](http://www.js.1989), 89, 375–382.
- (2) Anderson, J. L. *COLLOID TRANSPORT BY INTERFACIAL FORCES*; 1989; Vol. 21.
- (3) Howse, J. R.; Jones, R. A. L.; Ryan, A. J.; Gough, T.; Vafabakhsh, R.; Golestanian, R. Self-Motile Colloidal Particles: From Directed Propulsion to Random Walk. *Phys. Rev. Lett.* **2007**, 99 (4), 8–11. <https://doi.org/10.1103/PhysRevLett.99.048102>.
- (4) Golestanian, R.; Liverpool, T. B.; Ajdari, A. Propulsion of a Molecular Machine by Asymmetric Distribution of Reaction Products. *Phys. Rev. Lett.* **2005**, 94 (22), 1–4. <https://doi.org/10.1103/PhysRevLett.94.220801>.
- (5) Palacci, J.; Sacanna, S.; Steinberg, A. P.; Pine, D. J.; Chaikin, P. M. Colloidal Surfers. *Science (80-.)*. **2013**, 339 (February), 936–939.
- (6) Paxton, W. F.; Kistler, K. C.; Olmeda, C. C.; Sen, A.; St. Angelo, S. K.; Cao, Y.; Mallouk, T. E.; Lammert, P. E.; Crespi, V. H. Catalytic Nanomotors: Autonomous Movement of Striped Nanorods. *J. Am. Chem. Soc.* **2004**, 126 (41), 13424–13431. <https://doi.org/10.1021/ja047697z>.
- (7) Brooks, A. M.; Tasinkevych, M.; Sabrina, S.; Velegol, D.; Sen, A.; Bishop, K. J. M. Shape-Directed Rotation of Homogeneous Micromotors via Catalytic Self-Electrophoresis. *Nat. Commun.* **2019**, 10 (1), 1–9. <https://doi.org/10.1038/s41467-019-08423-7>.
- (8) Jin, C.; Krüger, C.; Maass, C. C. Chemotaxis and Autochemotaxis of Self-Propelling Droplet Swimmers. *Proc. Natl. Acad. Sci.* **2017**, 114 (20), 5089–5094. <https://doi.org/10.1073/pnas.1619783114>.

- (9) Popescu, M. N.; Uspal, W. E.; Bechinger, C.; Fischer, P. Chemotaxis of Active Janus Nanoparticles. *Nano Lett.* **2018**, *18* (9), 5345–5349. <https://doi.org/10.1021/acs.nanolett.8b02572>.
- (10) Dwivedi, P.; Shrivastava, A.; Pillai, D.; Mangal, R. Rheotaxis of Active Droplets. *Phys. Fluids* **2021**, *33* (8). <https://doi.org/10.1063/5.0060952>.
- (11) Si, B. R.; Patel, P.; Mangal, R. Self-Propelled Janus Colloids in Shear Flow. *Langmuir* **2020**, *36* (40), 11888–11898. <https://doi.org/10.1021/acs.langmuir.0c01924>.
- (12) Palacci, J.; Sacanna, S.; Abramian, A.; Barral, J.; Hanson, K.; Grosberg, A. Y.; Pine, D. J.; Chaikin, P. M. Artificial Rheotaxis. *Sci. Adv.* **2015**, *1* (4), 1–7. <https://doi.org/10.1126/sciadv.1400214>.
- (13) Uspal, W. E.; Popescu, M. N.; Dietrich, S.; Tasinkevych, M. Rheotaxis of Spherical Active Particles near a Planar Wall. *Soft Matter* **2015**, *11* (33), 6613–6632. <https://doi.org/10.1039/C5SM01088H>.
- (14) Ten Hagen, B.; Kümmel, F.; Wittkowski, R.; Takagi, D.; Löwen, H.; Bechinger, C. Gravitaxis of Asymmetric Self-Propelled Colloidal Particles. *Nat. Commun.* **2014**, *5*. <https://doi.org/10.1038/ncomms5829>.
- (15) Thutupalli, S.; Seemann, R.; Herminghaus, S. Swarming Behavior of Simple Model Squirmer. *New J. Phys.* **2011**, *13*, 0–10. <https://doi.org/10.1088/1367-2630/13/7/073021>.
- (16) Kitahata, H.; Yoshinaga, N.; Nagai, K. H.; Sumino, Y. Spontaneous Motion of a Droplet Coupled with a Chemical Wave. *Phys. Rev. E - Stat. Nonlinear, Soft Matter Phys.* **2011**, *84* (1). <https://doi.org/10.1103/PhysRevE.84.015101>.
- (17) Hirono, A.; Toyota, T.; Asakura, K.; Banno, T. Locomotion Mode of Micrometer-Sized Oil Droplets in Solutions of Cationic Surfactants Having Ester or Ether Linkages. *Langmuir* **2018**, *34* (26), 7821–7826. <https://doi.org/10.1021/acs.langmuir.8b01352>.
- (18) Thakur, S.; Kumar, P. B. S.; Madhusudana, N. V.; Pullarkat, P. A. Self-Propulsion of Nematic Drops: Novel Phase Separation Dynamics in Impurity-Doped Nematogens. *Phys. Rev. Lett.* **2006**, *97* (11), 21–24. <https://doi.org/10.1103/PhysRevLett.97.115701>.
- (19) Dwivedi, P.; Si, B. R.; Pillai, D.; Mangal, R. Solute Induced Jittery Motion of Self-

- Propelled Droplets Solute Induced Jittery Motion of Self-Propelled Droplets. **2021**, *022103* (January). <https://doi.org/10.1063/5.0038716>.
- (20) Izri, Z.; Van Der Linden, M. N.; Michelin, S.; Dauchot, O. Self-Propulsion of Pure Water Droplets by Spontaneous Marangoni-Stress-Driven Motion. *Phys. Rev. Lett.* **2014**, *113* (24). <https://doi.org/10.1103/PhysRevLett.113.248302>.
- (21) Izzet, A.; Moerman, P.; Groenewold, J.; Bibette, J.; Brujić, J. Tunable Active Rotational Diffusion in Swimming Droplets. **2019**, 1–7.
- (22) Morozov, M.; Michelin, S. Nonlinear Dynamics of a Chemically-Active Drop: From Steady to Chaotic Self-Propulsion. *J. Chem. Phys.* **2019**, *150* (4). <https://doi.org/10.1063/1.5080539>.
- (23) Suda, S.; Suda, T.; Ohmura, T.; Ichikawa, M. Straight-to-Curvilinear Motion Transition of a Swimming Droplet Caused by the Susceptibility to Fluctuations. *Phys. Rev. Lett.* **2021**, *127* (8), 88005. <https://doi.org/10.1103/PhysRevLett.127.088005>.
- (24) Krüger, C.; Klös, G.; Bahr, C.; Maass, C. C. Curling Liquid Crystal Microswimmers: A Cascade of Spontaneous Symmetry Breaking. *Phys. Rev. Lett.* **2016**, *117* (4), 1–5. <https://doi.org/10.1103/PhysRevLett.117.048003>.
- (25) Krüger, C.; Klös, G.; Bahr, C.; Maass, C. C. Curling Liquid Crystal Microswimmers: A Cascade of Spontaneous Symmetry Breaking. *Phys. Rev. Lett.* **2016**, *117* (4). <https://doi.org/10.1103/PhysRevLett.117.048003>.
- (26) Hokmabad, B. V.; Dey, R.; Jalaal, M.; Mohanty, D.; Almukambetova, M.; Baldwin, K. A.; Lohse, D.; Maass, C. C. Emergence of Bimodal Motility in Active Droplets. *Phys. Rev. X* **2021**, *11* (1), 1–19. <https://doi.org/10.1103/PhysRevX.11.011043>.
- (27) Hokmabad, B. V.; Dey, R.; Jalaal, M.; Mohanty, D.; Almukambetova, M.; Baldwin, K. A.; Lohse, D.; Maass, C. C. Emergence of Bimodal Motility in Active Droplets. *arXiv:2005.12721v2* **2020**.
- (28) Morozov, M.; Michelin, S. Nonlinear Dynamics of a Chemically-Active Drop: From Steady to Chaotic Self-Propulsion. *J. Chem. Phys.* **2019**, *150* (4). <https://doi.org/10.1063/1.5080539>.

- (29) Michelin, S.; Lauga, E.; Bartolo, D. Spontaneous Autophoretic Motion of Isotropic Particles. *Phys. Fluids* **2013**, *25* (6). <https://doi.org/10.1063/1.4810749>.
- (30) Morozov, M. Adsorption Inhibition by Swollen Micelles May Cause Multistability in Active Droplets. *Soft Matter* **2020**, *16* (24), 5624–5632. <https://doi.org/10.1039/d0sm00662a>.
- (31) Cai, L. H.; Panyukov, S.; Rubinstein, M. Mobility of Nonsticky Nanoparticles in Polymer Liquids. *Macromolecules* **2011**, *44* (19), 7853–7863. <https://doi.org/10.1021/ma201583q>.
- (32) Yamamoto, U.; Schweizer, K. S. Microscopic Theory of the Long-Time Diffusivity and Intermediate-Time Anomalous Transport of a Nanoparticle in Polymer Melts. *Macromolecules* **2015**, *48* (1), 152–163. <https://doi.org/10.1021/ma501150q>.
- (33) Kalathi, J. T.; Yamamoto, U.; Schweizer, K. S.; Grest, G. S.; Kumar, S. K. Nanoparticle Diffusion in Polymer Nanocomposites. *Phys. Rev. Lett.* **2014**, *112* (10), 1–5. <https://doi.org/10.1103/PhysRevLett.112.108301>.
- (34) Mangal, R.; Srivastava, S.; Archer, L. A. Phase Stability and Dynamics of Entangled Polymer-Nanoparticle Composites. *Nat. Commun.* **2015**, *6*, 1–9. <https://doi.org/10.1038/ncomms8198>.
- (35) Mangal, R.; Srivastava, S.; Narayanan, S.; Archer, L. A. Size-Dependent Particle Dynamics in Entangled Polymer Nanocomposites. *Langmuir* **2016**, *32* (2), 596–603. <https://doi.org/10.1021/acs.langmuir.5b03311>.
- (36) Nath, P.; Mangal, R.; Kohle, F.; Choudhury, S.; Narayanan, S.; Wiesner, U.; Archer, L. A. Dynamics of Nanoparticles in Entangled Polymer Solutions. *Langmuir* **2018**, *34* (1), 241–249. <https://doi.org/10.1021/acs.langmuir.7b03418>.
- (37) Zhu, L.; Lauga, E.; Brandt, L. Self-Propulsion in Viscoelastic Fluids: Pushers vs. Pullers. *Phys. Fluids* **2012**, *24* (5). <https://doi.org/10.1063/1.4718446>.
- (38) Lighthill, M. J. On the Squirming Motion of Nearly Spherical Deformable Bodies through Liquids at Very Small Reynolds Numbers. *Commun. Pure Appl. Math.* **1952**, *5* (2), 109–118. <https://doi.org/10.1002/cpa.3160050201>.
- (39) Blake, J. R. A Spherical Envelope Approach to Ciliary Propulsion. *J. Fluid Mech.* **1971**, *46*

- (1), 199–208. <https://doi.org/10.1017/S002211207100048X>.
- (40) Pedley, T. J. Spherical Squirmer: Models for Swimming Micro-Organisms. *IMA J. Appl. Math. (Institute Math. Its Appl.* **2016**, *81* (3), 488–521.
<https://doi.org/10.1093/imamat/hxw030>.
- (41) Li, G. Swimming Dynamics of a Self-Propelled Droplet. *J. Fluid Mech.* **2022**, *934*, 1–15.
<https://doi.org/10.1017/jfm.2021.1154>.
- (42) De Corato, M.; Greco, F.; Maffettone, P. L. Locomotion of a Microorganism in Weakly Viscoelastic Liquids. *Phys. Rev. E - Stat. Nonlinear, Soft Matter Phys.* **2015**, *92* (5).
<https://doi.org/10.1103/PhysRevE.92.053008>.